Previous Article

February 2014
Volume 270, Issue 2

Next Article

Original Research
Neuroradiology

White Matter Changes in Comatose Survivors of Anoxic Ischemic Encephalopathy and Traumatic Brain Injury: Comparative Diffusion-Tensor Imaging Study

Anke W. van der Eerden, MD, Omid Khalilzadeh, MD, MPH, Vincent Perlbarg, PhD, Julien Dinkel, MD, PhD, Paola Sanchez, MD, Pieter E. Vos, MD, PhD, Charles-Edouard Luyt, MD, PhD, Robert D. Stevens, MD, PhD, Nicolas Menjot de Champfleur, MD, PhD, Christine Delmaire, MD, Eleonore Tollard, MD, Rajiv Gupta, MD, PhD, Didier Dormont, MD, PhD, Steven Laureys, MD, PhD, Habib Benali, MD, PhD, Audrey Vanhaudenhuyse, PhD, Damien Galanaud, MD, PhD, Louis PuybassetFor the NICER (Neuro Imaging for Coma Emergence and Recovery) Consortium, MD, PhD,

From the Department of Neuroradiology (A.W.v.d.E., D.D., D.G.), the Neurosurgical ICU (P.S., L.P.), and the Medical ICU (C.E.L.), Hôpital Pitié-Salpêtrière, Assistance Publique–Hôpitaux de Paris, 47-83 boulevard de l'Hôpital, 75651 Paris Cedex 13, France; Departments of Radiology (A.W.v.d.E.) and Neurology (P.E.V.), Radboud University Nijmegen Medical Centre, Nijmegen, the Netherlands; INSERM, UMRS 678, Université Pierre et Marie Curie-Paris 6, Paris, France (V.P., H.B.); Department of Radiology, Massachusetts General Hospital, Boston, Mass (O.K., J.D., R.G.); Division of Neuroscience Critical Care, Department of Anesthesiology Critical Care Medicine, Johns Hopkins University School of Medicine, Baltimore, Md (R.D.S.); Department of Neuroradiology, Guy de Chauliac Hospital, Montpellier, France (N.M.d.C.); Department of Neuroradiology, Roger Salengro Hospital, Lille, France (C.D.); Department of Neuroradiology, Centre Hospitalier Universitaire, Rouen, France (E.T.); and Cyclotron Research Center, University of Liège, Liège, Belgium (S.L., A.V.).

DOI: http://dx.doi.org/10.1148/radiol.13122720

Show Conflicts of Interest and Funding

Show Author Contribution

Show Abbreviations

Cardiac arrest and traumatic brain injury (TBI) may lead to similar clinical presentations that include prolonged impaired consciousness, even though these two types of insult have vastly different pathophysiologic mechanisms. These differences are reflected in the spatial distribution of abnormalities over the brain. In TBI, shearing and acceleration-deceleration forces lead to diffuse axonal injury mostly in the central structures such as the brainstem and corpus callosum, often associated with contusions in the cerebral hemispheres (1). In cardiac arrest, the areas most vulnerable to damage are the watershed areas of the cerebral hemispheres (2–4).

Diffusion-tensor (DT) imaging provides information not only on lesion localization but also on the nature of white matter damage. The DT imaging parameter axial diffusivity (λ_1) depends chiefly on the diffusibility of water molecules parallel to a tract, whereas radial diffusivity ($\lambda_\perp$) assesses water diffusion perpendicular to the tract (5). Thus, changes in λ_1 are thought to be associated primarily with axonal damage, while changes in $\lambda_\perp$ are thought to relate to myelin injury (6–8). These parameters provide greater anatomic and functional information than scalar DT imaging parameters such as fractional anisotropy and the apparent diffusion coefficient (6,9–13), which have been more extensively evaluated than λ_1 and $\lambda_\perp$. These constructs have been validated in animal models (6–8,14,15). Their meaning in humans has been less studied.

We hypothesized that the different pathophysiologic events occurring in the subacute phase after cardiac arrest and TBI have different effects on λ_1 and $\lambda_\perp$. The purpose of this study was to analyze the anatomic distribution of white matter pathologic abnormalities by using DT imaging in a multicenter prospective cohort of patients with impaired consciousness following cardiac arrest or TBI.

Materials and Methods

Section: Choose

The institutional review boards of the participating institutions approved this prospective study. All patients' next of kin and healthy control subjects gave informed consent. The patients and healthy control subjects were recruited during a study on the relevance of DT imaging biomarkers in the prediction of recovery of consciousness in patients after cardiac arrest and after TBI. In that study, the researchers used the same inclusion and exclusion criteria, the same clinical data and the same methods of magnetic resonance

Article Tools

Open in Image Viewer
Add to myRSNA
Add to Favorites
Email to a Friend
Download Citation
Track Citations
Rights & Permissions

Related Articles

MR Imaging for Diagnostic Evaluation of Encephalopathy in the Newborn
Shroff et al. *RadioGraphics.* (2010)

Admission Perfusion CT: Prognostic Value in Patients with Severe Head Trauma
Wintermark et al. *Radiology.* (2004)

Diffusion-Tensor Fiber Tractography: Intraindividual Comparison of 3.0-T and 1.5-T MR Imaging
Okada et al. *Radiology.* (2006)

Imaging of Acute Cerebral Ischemia
Beauchamp et al. *Radiology.* (1999)

Infants with Perinatal Hypoxic Ischemia: Feasibility of Fiber Tracking at Birth and 3 Months
van Pul et al. *Radiology.* (2006)

See More

Original Research

Breast Imaging
Cardiac Imaging
Computer Applications
Contrast Media
Emergency Radiology
Evidence-based Practice
Experimental Studies
Gastrointestinal Imaging
Genitourinary Imaging
Head and Neck Imaging
Health Policy and Practice
Medical Physics
Molecular Imaging
Musculoskeletal Imaging
Neuroradiology
Nuclear Medicine
Obstetric Imaging
Pediatric Imaging

(MR) imaging acquisition and MR imaging analysis as were used in the present study. The study on the relevance of DT imaging biomarkers in the prediction of recovery of consciousness led to two articles, one for cardiac arrest (16) and the other for TBI (17), and the design is reported in more detail in those two previous articles (16,17). Two authors (V.P., a computer scientist with 10 years of experience, and D.G., a neuroradiologist with 15 years of experience) processed the DT imaging acquisitions. They had no access to the clinical information and outcome of the patients.

Patients

Consecutive patients were enrolled prospectively in eight intensive care units in Paris, Lille, Lyon, Montpellier, Nancy, Rouen, and Bordeaux in France and in Liège in Belgium following cardiac arrest or TBI between October 2006 and February 2010. Patients were eligible if they *(a)* were between 18 and 85 years old, and *(b)* had severe brain damage, as expressed by *(i)* inability to follow simple commands 7–28 days after the incident, unexplained by sedation, and *(ii)* a Glasgow Outcome Scale (18) score of 1 or 2 at 12 months after the injury or a Glasgow Outcome Scale score of 3 that was explained by cognitive and not purely physical impairment. On the basis of these inclusion criteria, 57 patients with cardiac arrest and 55 patients with TBI were eligible. Patients were excluded if they *(a)* had a central neurologic disease prior to cardiac arrest or TBI (n = 2); *(b)* had a penetrating head injury (n = 1); *(c)* were moribund (expected survival of < 24 hours) (n = 0); *(d)* had a contraindication to MR imaging (*n* = 4); or *(e)* were too unstable to be transported and to undergo MR imaging (*n* = 0). On the basis of their eligibility, we enrolled 54 patients with cardiac arrest and 51 patients with TBI. Of these, the MR imaging data in five patients with cardiac arrest and in 11 patients with TBI could not be evaluated because of a suboptimal MR imaging acquisition, as a result of motion (four cardiac arrest patients, five TBI patients), other artifacts (zero cardiac arrest patients, one TBI patient), or deviation in the MR imaging protocol (one cardiac arrest patient, one TBI patient), or because an insufficient number of healthy control subjects were imaged (zero cardiac arrest patients, four TBI patients). Finally, we included 49 of 57 patients with cardiac arrest (86%) and 40 of 55 patients with TBI (73%) with sufficient quality normalized DT imaging data. Demographic and clinical characteristics of the patients are summarized in Table 1.

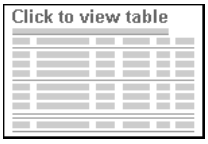

Table 1. Demographics and Clinical Characteristics of the Patients

Cardiac Arrest

The cause of the cardiac arrest was primarily cardiac (cardiac arrest originating in the heart [eg, myocardial infarction]) in 39 of 49 patients (80%) and secondarily cardiac (cardiac arrest resulting from disease outside the heart [eg, severe hypoxia or hyperkalemia]) in 10 of 49 patients (20%). The mean duration of no flow before cardiopulmonary resuscitation was 5 minutes (interquartile range, 0–10 minutes). It took a median of 20 minutes (interquartile range, 10–36 minutes) for the circulation to become fully effective under cardiopulmonary resuscitation. Hypothermia was induced in 29 of 49 patients (59%). At admission, the mean serum troponin I level was 0.48 ng/mL (0.48 μg/L), with an interquartile range of 0.1–4.4 ng/mL (0.1–4.4 μg/L).

Traumatic Brain Injury

TBI was caused by a motor vehicle accident in 26 of 40 cases (65%) (20 drivers or passengers [50%] and six pedestrians [15%]), by a fall in nine of 40 cases (23%), and by another mechanism in five of 40 cases (13%). On a computed tomography (CT) scan obtained within 48 hours of the TBI, six of 40 TBI patients (15%) had an epidural hematoma, 14 of 40 patients (35%) had a subdural hematoma, 34 of 40 patients (85%) had a subarachnoid hemorrhage, 27 of 40 patients (68%) had one or more contusions, and nine of 40 patients (23%) had a midline shift larger than 6 mm. None of the TBI patients had signs of ischemia on this early CT scan. Of 40 patients, 18 (45%) had a Marshall classification diffuse injury I–II, five (13%) had a Marshall classification diffuse injury III, one (3%) had a Marshall classification diffuse injury IV, and 15 (38%) had a mass lesion (eight patients had an evacuated mass lesion and seven patients had a nonevacuated mass lesion) (19). Fourteen of 40 TBI patients (35%) underwent a neurosurgical intervention.

Healthy Control Subjects

To control for multisite variability in DT imaging data, in each center we compared the patients' DT imaging values with those of a total of 111 healthy volunteers, with four to 51 control subjects per center; 60 of 111 (54%) were men and 51 (46%) were women (mean age, 33 years ± 3 [standard deviation]). These control subjects underwent MR imaging with the same acquisition parameters as the patients. Volunteers were recruited by the local principal investigator among staff members of each center. They gave written informed consent to study participation. Individuals with no history of neurologic disease requiring medical attention were eligible. We excluded volunteers with abnormalities in the morphologic sequences, as occurred in two individuals (two of 113, 2%): one with mild atrophy and another with asymptomatic white matter disease.

Clinical Data Collection

Data were prospectively collected by using standardized case report forms and a Web-based, encrypted, and centrally managed data management system. Specific data included the following: patient demographics; initial clinical status and cranial CT scan; and 1-year outcome, including the Glasgow Outcome Scale score on a five-point scale (18) and cognitive and physical impairment as assessed by the investigating team at each participating center via a telephone interview or via an in-person visit. A central study monitor verified all data for accuracy, consistency, and completeness.

MR Imaging Acquisition

MR imaging was performed after enrollment and as soon as MR imaging was clinically feasible, which was a mean of 23.2 days ± 1.7 (range, 7–57 days) after TBI and a mean of 13.1 days ± 1.2 (range, 5–47 days) after cardiac arrest. Vital signs were continuously monitored during imaging. Sedation, if any, was maintained. MR imaging was performed in eight centers using nine imaging units from three manufacturers (Siemens [Erlangen, Germany], GE Healthcare [Milwaukee, Wis], and Philips Healthcare [Eindhoven, the Netherlands]) and included units with both 1.5- and 3.0-T magnetic field strength. The imaging protocol has been described in previous publications (16,17). The DT imaging acquisition parameters were optimized for each MR unit, with minimal specifications of a pixel size of at most 3 × 3 × 3 mm, a *B* value of 1000 mT/m, and at least 12 gradient directions. The clinical team did not have access to the DT imaging results, while the investigators processing the DT imaging acquisitions (V.P. and D.G.) had no access to the clinical information and outcome of the patients. No adverse events related to MR imaging were reported.

Radiation Oncology
Special Reports
Technical Developments
Thoracic Imaging
Ultrasonography
Vascular/Interventional Radiology

MR Imaging Analysis

The pre- and postprocessing of the DT imaging data are described in Appendix E1 (online). This process uses nonlinear registration of λ_1 and $\lambda_\perp$ maps into a standard space, as implemented in software (FLIRT/FNIRT procedures; FSL Software Technologies, New Delhi, India). The averaged λ_1 and $\lambda_\perp$ values were then extracted in 19 predefined white matter regions of interest (ROIs) (Fig 1), which were selected from the white matter atlas (20). To account for intercenter and intersequence variability, these values were normalized to values of healthy control subjects by scaling each value of a patient to the mean of the corresponding parameter calculated from the healthy control subjects who underwent imaging by using the same acquisition parameters in the same center, as previously described (16,17). We tested the effects of three factors (acquisition/center, ROIs, groups) on the mean of the regional fractional anisotropy calculated in the patients and control subjects by using a three-way analysis of variance. The results showed that, before normalization, the three factors were significant ($P < .05$), and after normalization, only the group effect significantly explained the data variability. We did not adjust for the center-specific standard deviation. The intrasite coefficient of variation (ratio of the standard deviation and the mean) ranged from 2% (within the splenium of the corpus callosum) to 10% (within the body of the corpus callosum) with homogeneous variance across centers (Bartlett test). For explorative analyses, the 19 ROIs were gathered into five groups: lower brainstem region, cerebral peduncles region, corpus callosum region, right hemisphere, and left hemisphere (Fig 1). The statistical analyses of raw MR data were performed by a computer scientist (V.P., with 10 years of experience) and a mathematician (H.B., with 30 years of experience). Image analysis and quality control of MR images were performed by two neuroradiologists (D.G., with 15 years of experience, and E.T., with 10 years of experience). Data consistency and data integrity were checked by an anesthesiologist (L.P., with 20 years of experience).

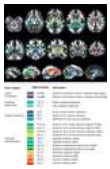

Figure 1:. Automatically segmented white matter ROIs for measurement of DT imaging parameters. The background images are the FMRIB58–fractional anisotropy standard space images provided in FSL. The ROIs defined by Mori et al (20) are color coded and superimposed on these background fractional anisotropy images. For explorative analyses, the color-coded ROIs in the anterior and posterior brainstem were collapsed into a single lower brainstem region; the ROIs in the cerebral peduncles were collapsed into a single cerebral peduncles region; the ROIs in the genu, splenium, and body of the corpus callosum were collapsed into a single corpus callosum region; and the ROIs in the paired anterior and posterior limbs of the internal capsule, sagittal stratum, superior longitudinal fasciculus, external capsule, and corona radiata were collapsed into right hemisphere and left hemisphere regions.

Open in Image Viewer

Statistical Analysis

Data were analyzed by using statistical software (StatView 5.0, SAS Institute, Cary, NC; and SPSS 18, SPSS, Chicago, Ill). Values are expressed as means and standard errors of the mean unless otherwise stated. Differences in demographic and clinical variables were tested by using the Student *t* test and the χ^2 test, as appropriate. DT imaging variables had normal distribution (according to the Kolmogorov-Smirnov test); therefore, we used parametric tests. We used the method of general linear modeling (analysis of variance with Bonferroni post hoc) for within- and between-group comparison of DT imaging variables in healthy control subjects, TBI patients, and cardiac arrest patients. Multivariate analyses were performed to evaluate the results after adjustment for age and sex. The interaction between variables was also assessed. We calculated Pearson correlation coefficients between the DT imaging parameters in each left-sided ROI and the corresponding right-sided ROI. *P* values were corrected for multiple testing by multiplication of the *P* values by the number of tested hypotheses; for example, *P* values were multiplied by 19 when we compared DT imaging values among the groups in the 19 ROIs (Bonferroni method). Throughout the article, we present the corrected *P* values. A difference with a corrected value of $P < .05$ was considered significant.

Results

Section: *Choose*

The λ_1 and $\lambda_\perp$ values in various brain regions of patients and healthy control subjects are illustrated in Figures 2–5.

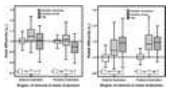

Figure 2:. Normalized values of λ_1 and $\lambda_\perp$ in the lower brainstem region of patients and healthy control subjects. Box plots show the median (middle horizontal line in each box), interquartile range (25th [bottom of box] to 75th [top of box] quartiles), and the minimum (bottom of whisker) and maximum (top of whisker) values. Asterisks = *P* values for within- and between-group comparisons. When the combined ROIs were compared, *P* values with significant differences were as follows: For λ_1, TBI versus cardiac arrest patients, $P < .01$; for λ_1 and $\lambda_\perp$, TBI versus healthy control subjects and cardiac arrest patients versus healthy control subjects, $P < .01$. There were no significant interactions between the anterior and posterior brainstem. * = $P < .05$, ** = $P < .01$, NS = not significant.

Open in Image Viewer

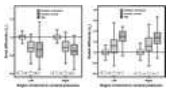

Figure 3:. Normalized values of λ_1 and $\lambda_\perp$ in the cerebral peduncles region of patients and healthy control subjects. Box plots show the median (middle horizontal line in each box), interquartile range (25th [bottom of box] to 75th [top of box] quartiles), and the minimum (bottom of whisker) and maximum (top of whisker) values. Asterisks = *P* values for within- and between-group comparisons. When the combined ROIs were compared, *P* values with significant differences were as follows: For $\lambda_\perp$, TBI versus cardiac arrest patients, $P < .01$; for λ_1 and $\lambda_\perp$, TBI patients versus healthy control subjects and cardiac arrest patients versus healthy control subjects, $P < .01$. There were no significant interactions between the left and the right cerebral peduncles. ** = $P < .01$, NS = not significant.

Open in Image Viewer

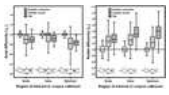

Figure 4:. Normalized values of λ_1 and $\lambda_\perp$ in the corpus callosum region of patients after TBI, of patients after cardiac arrest, and of healthy control subjects. Box plots show the median (middle horizontal line in each box), interquartile range (25th [bottom of box] to 75th [top of box] quartiles), and the minimum (bottom of whisker) and maximum (top of whisker) values. Asterisks = *P* values for within- and between-group comparisons. When the combined ROIs were compared, *P* values with significant differences were as follows: For $\lambda_\perp$, TBI versus cardiac arrest patients, $P < .01$; for λ_1 and $\lambda_\perp$, TBI patient versus healthy control subjects and cardiac arrest patients versus healthy control subjects, $P < .01$. For interaction between the splenium, body, and genu for λ_1, $P < .05$, and for $\lambda_\perp$, $P < .01$. ** = $P < .01$, NS = not significant.

Open in Image Viewer

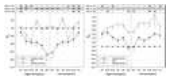

Figure 5:. Normalized values of λ_1 and $\lambda_\perp$ in the cerebral hemispheres of patients and healthy control subjects. The right hemisphere is at left, and the left hemisphere is at right. Asterisks = *P* values for within- and between-group comparisons. Symbols in each line = mean for each member of the group indicated; error bars = standard errors of the mean. For interaction between the ROIs in the right hemisphere for both λ_1 and $\lambda_\perp$, $P < .01$; for interaction between the ROIs in the left hemisphere for λ_1, $P < .01$. Notice the symmetrical pattern of involvement for λ_1 in TBI and cardiac arrest patients and for $\lambda_\perp$ in cardiac arrest patients, while the pattern of involvement for $\lambda_\perp$ in TBI patients is asymmetric. * = $P < .05$, ** = $P < .01$, *ALIC* = anterior limb of internal capsule, *CA* = cardiac arrest, *CR* = corona radiata, *Ctrl* = healthy control subject, *EC* = external capsule, *NS* = not significant, *PLIC* = posterior limb of internal capsule, *SLF* = superior longitudinal fasciculus, *SS* = sagittal stratum.

Open in Image Viewer

λ_1 and $\lambda_\perp$ in Patients versus Healthy Control Subjects

The λ_1 and $\lambda_\perp$ in the anterior brainstem and $\lambda_\perp$ in the posterior brainstem were higher in cardiac arrest patients than in control subjects (all $P < .01$). The λ_1 was lower in the posterior brainstem, and $\lambda_\perp$ was higher in the posterior brainstem and in the anterior brainstem in TBI patients compared with control subjects (all $P < .01$) (Fig 2). The λ_1 was lower ($P < .05$) and $\lambda_\perp$ was higher ($P < .05$) in TBI patients and cardiac arrest patients than in control subjects in the left and right cerebral peduncles, body, genu, and splenium of the corpus callosum (except for λ_1 in the genu) (Figs 3, 4). Thus, in central white matter, λ_1 differed from that in control subjects in six of seven TBI ROIs and five of seven cardiac arrest ROIs (all $P < .01$). The $\lambda_\perp$ differed from that in control subjects in all ROIs in both patient groups ($P < .01$) (Figs 2–4). For the various ROIs in the cerebral hemispheres, Figure 5 shows the comparison of λ_1 and $\lambda_\perp$ in patients versus in control subjects. Thus, in hemispheres, λ_1 was decreased compared with that in control subjects in three of 12 TBI ROIs ($P < .05$) and nine of 12 cardiac arrest ROIs ($P < .01$). The $\lambda_\perp$ was increased in all TBI ROIs ($P < .01$) and in seven of 12 cardiac arrest ROIs ($P < .05$). Cerebral hemisphere λ_1 was lower in cardiac arrest than in TBI in six of 12 ROIs ($P < .01$), while $\lambda_\perp$ was higher in TBI than in cardiac arrest in eight of 12 ROIs ($P < .01$).

λ_1 and $\lambda_\perp$ in Cardiac Arrest versus TBI Patients

The major findings for the difference in λ_1 and $\lambda_\perp$ between TBI and cardiac arrest patients are reported in Figures 2–5. Table 2 presents the type and distribution of abnormalities in central regions (anterior and posterior brainstem, left and right cerebral peduncles, genu, body, and splenium of the corpus callosum) and in cerebral hemispheric regions (left and right sagittal strata, superior longitudinal fasciculus, anterior and posterior limb of internal capsule, external capsule, and corona radiata). In both central regions and cerebral hemispheres, $\lambda_\perp$ was higher ($P < .05$) in TBI patients than in cardiac arrest patients. In cerebral hemispheres, λ_1 was lower ($P < .05$) in cardiac arrest patients than in TBI patients.

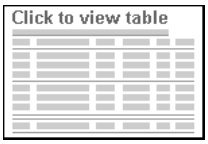

Table 2. Types and Distribution of Abnormalities in TBI and Cardiac Arrest Patients

The differences presented in Figures 2–4 remained significant after adjustment for age and sex.

λ_1 and $\lambda_\perp$ in the Left versus the Right Cerebral Hemisphere

Figure 5 shows a symmetrical pattern of DT imaging changes in the ROIs in the corresponding right and left hemispheres in patients with cardiac arrest and in control subjects. Indeed, there was a significant intercorrelation between DT imaging values of the ROIs in the corresponding right and left hemispheres in cardiac arrest patients (ranging from $r = 0.81$ in the external capsule to $r = 0.99$ in the corona radiata for λ_1 and from $r = 0.73$ in the external capsule to $r = 0.99$ in the corona radiata for $\lambda_\perp$; $P < .001$) and in control subjects (ranging from $r = 0.73$ in the sagittal stratum to $r = 0.84$ in the anterior limb of the internal capsule for λ_1 and from $r = 0.75$ in the external capsule to $r = 0.93$ in the corona radiata for $\lambda_\perp$; $P < .001$; values close to one represent symmetry between DT imaging values in the ROIs in the corresponding left and right hemispheres). In TBI patients, this symmetrical pattern of DT imaging changes was not seen for most ROIs (Table 3).

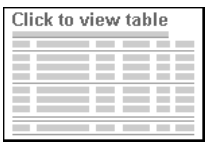

Table 3. Intercorrelations between DT Imaging Values in Corresponding ROIs in the Left and Right Hemispheres

Discussion

This article shows that DT imaging can help distinguish the different pathophysiologic mechanisms that underly similar states of impaired consciousness following TBI and cardiac arrest.

Our main findings are a marked decrease in λ_1 in cardiac arrest patients and a marked increase in $\lambda_\perp$ in TBI patients. These findings are consistent with reported pathophysiologic concepts, a fact that supports the validity of DT imaging to help distinguish axonal and myelin damage in vivo in groups of patients. Thus, in cardiac arrest, the marked decrease in λ_1 is consistent with primary axonal damage (6,10–13) related to energy depletion from anoxic ischemia. Primary axonal damage induces changes in the fluid microenvironment of the central nervous system, to which in turn myelin is susceptible (21–24). The moderate $\lambda_\perp$ increases in our cardiac arrest patients are consistent with such secondary myelin damage (25). Conversely, the marked $\lambda_\perp$ increase in many areas of TBI patients suggests myelin damage, edema, and/or macrophage infiltration as the primary injury. The mechanical forces exerted on the brain in TBI probably cause more myelin damage than axonal damage. The smaller λ_1 decrease in TBI patients is consistent with axonal damage, caused either by direct trauma (axonotmesis) or by indirect ischemic damage secondary to extracranial traumatic injuries. In a later phase, brain swelling and increased intracranial pressure may further contribute to the axonal damage. In cardiac arrest, there is a gradient of injury severity from the cerebral hemispheres toward the medulla oblongata, with relative sparing of the central brain structures (26). The vascular anatomy in the cerebral hemispheres, characterized by widespread linear arterioles with few anastomoses, increases the vulnerability of the hemispheric white matter to hypoxic-ischemic injury (27–29). Conversely, in TBI patients, $\lambda_\perp$ was highly abnormal in both the central brain structures and the cerebral hemispheres. This finding is consistent with the distribution of diffuse axonal injury observed in the classic monkey model of axial trauma caused by rotational and acceleration-deceleration shearing forces (30). The $\lambda_\perp$ increase and, to a lesser extent, the λ_1 decrease were asymmetric, being more pronounced in the left cerebral hemisphere of our TBI patients. This predominance of left-sided abnormalities in TBI patients with poor clinical outcomes was expected, as left-sided lesions are more frequently symptomatic. The asymmetry was attributable to a left predominance of $\lambda_\perp$ abnormalities and, to a lesser extent, λ_1 abnormalities, suggesting greater asymmetry of edema and/or myelin damage than of axonal damage. This finding supports the hypothesis that edema and myelin damage are chiefly related to the mechanical trauma, which is an asymmetric assault, whereas axonal damage may be a combined effect of symmetric systemic processes and asymmetric local processes.

Our finding of greater $\lambda_\perp$ as compared with λ_1 alterations in TBI patients is consistent with DT imaging findings in the key experimental mouse model of brain injury by Mac Donald et al (10). The researchers in all previous descriptive DT imaging studies in humans at the early subacute phase of TBI evaluated a later or longer time window than we did in our study (31–36), included patients with milder brain injury (33,36–38), and/or did not specify separate diffusivity parameters in various ROIs (33,35,36,38,39). As intuitively expected, $\lambda_\perp$ values and therefore myelin damage played a larger role than λ_1 in a recent DT imaging–based and clinically based prognostic model in severe TBI (17). To our knowledge, no previous descriptive DT imaging studies in human cardiac arrest patients have been published.

To our knowledge, investigators in only one previous study (40) have compared the use of DT imaging in cardiac arrest patients versus TBI patients. Our finding of greater severity of central brain structure injury in TBI patients versus cardiac arrest patients is consistent with the findings in the comparative study at a later postinjury phase of Newcombe et al (40). Although an overall λ_1 decrease was our main finding in cardiac arrest patients, λ_1 in the lower brainstem and cerebral peduncles regions showed larger decreases in TBI than in cardiac arrest. Similarly, in a study of 30 patients with severe TBI evaluated 8 weeks after trauma, λ_1 was decreased and $\lambda_\perp$ was increased in the deep brain regions and brainstem (31,41). Whereas we found large differences in the cerebral hemispheres between cardiac arrest and TBI, Newcombe et al (40) found broadly similar DT imaging abnormalities in TBI and ischemic-hypoxic brain injury. This discrepancy is ascribable to differences in patient populations and MR imaging timing, as well as to the relatively small number of patients studied by Newcombe et al.

Our study had several limitations. As was inevitable with a multicenter design, the DT imaging data were acquired with different MR imaging machines. We corrected for this source of variability by normalizing the patient values to values in healthy control subjects who underwent imaging with the same parameters on the same machine. Because of the epidemiology of TBI and cardiac arrest, our TBI patients were younger and cardiac arrest patients had higher mortality rates. Differences in treatment-limitation decisions between the two patient groups cannot be ruled out. We followed up the patients for 1 year. Although improvements are unlikely to occur beyond this period, some degree of conformation bias cannot be ruled out. In both cardiac arrest and TBI, neurologic injury and recovery is a dynamic process. Therefore, our findings are only valid within the studied time (ie, the early subacute phase [42]). In TBI, the spatial distribution varies across patients as a result of variations in the direction of the impact on the head. That highly significant results were found in our study despite this inevitable source of heterogenity supports the general applicability of our findings.

Our results should be tested in future research evaluating the robustness and validity of λ_1 and $\lambda_\perp$, preferably comparing the DT imaging results with postmortem pathologic findings.

Although the neurologic presentation is similar in patients with persistent consciousness impairments after TBI and cardiac arrest, DT imaging findings suggest substantial differences in white matter injury between these two causes. Our findings indicate differences at both the topographic and the cellular levels. The results in cardiac arrest patients are consistent with a primary axonal injury responsible for secondary myelin damage. In TBI in contrast, the chiefly mechanical primary mechanism results in myelin damage, which is followed by secondary ischemic injury. The consistency of our findings with current pathophysiologic concepts supports the validity of DT imaging for in vivo testing of pathophysiologic hypotheses in humans. DT imaging is a promising in vivo tool for separating myelin from axonal damage, a step that may prove important in the early prediction and understanding of patient outcomes.

Advances in Knowledge

- In cardiac arrest, the predominant finding at diffusion-tensor (DT) imaging is a marked decrease in axial diffusivity (λ_1) (−8.9% in central regions, −9.1% in cerebral hemispheres), whereas in traumatic brain injury (TBI), the predominant finding is a marked increase in radial diffusivity ($\lambda_\perp$) (37.5% in central regions, 24.9% in cerebral hemispheres).

■ The central brain structures show lower λ_1 and higher $\lambda_\perp$ values in TBI than in cardiac arrest (cardiac arrest vs TBI, $P < .01$ for λ_1 in the lower brainstem region and for $\lambda_\perp$ in the cerebral peduncles region and corpus callosum region); in the cerebral hemispheres regions, λ_1 and $\lambda_\perp$ are highly abnormal in both cardiac arrest and TBI, with the lowest λ_1 values occurring in cardiac arrest (cardiac arrest vs TBI, −9.1% vs −0.1%; $P < .01$) and the highest $\lambda_\perp$ values in TBI (TBI vs cardiac arrest, 24.9% vs 9.7%; $P < .01$).

■ The known predominance of left-sided damage in TBI patients with poor clinical outcomes is attributable to left-sided predominance of $\lambda_\perp$ abnormalities and, to a lesser extent, λ_1 abnormalities ($P > .05$ for side-to-side correlations in five of six ROIs for $\lambda_\perp$ and in three of six ROIs for λ_1); this finding suggests greater asymmetry of edema and/or myelin damage than of axonal damage in TBI.

Implications for Patient Care

■ Our findings help physicians understand the mechanisms underlying chronic consciousness impairments after TBI and cardiac arrest.

■ Our findings encourage physicians who interpret DT imaging studies to take into account not only scalar variables such as fractional anisotropy and apparent diffusion coefficient but also vector variables such as λ_1 and $\lambda_\perp$.

Acknowledgment

We acknowledge Ritse Mann for editing Figures 2, 3, and 4.

Received December 18, 2012; revision requested February 20, 2013; final revision received May 20; accepted May 29; final version accepted August 12.

Supported by a grant from the French Ministry of Health (Projet Hospitalier de Recherche Clinique registration P051061 [2005]), Paris, France, and from the Agence Nationale de la Recherche, Paris France, for the program “investissements d’avenir” under agreement ANR-10-IAIHU-06 for the Paris Institute of Translational Neurosciences-IHU-A-ICM.

References

Section: Choose

1. Elovic E, Baerga E, Cuccurullo S. Mechanism and recovery of head injury. In: Cuccurullo S, ed. Physical medicine and rehabilitation board review. New York, NY: Demos Medical Publishing, 2004; http://www.ncbi.nlm.nih.gov/books/NBK27256/.
2. Ringelstein EB, Stogbauer F. Border zone infarcts. In: Bogousslavsky J, Caplan L, eds. Stroke syndromes. 2nd ed. Cambridge, England: Cambridge University Press, 2001; 564–582.
3. Lövblad KO. Hypoxic-ischemic Lesions. In: Von Kummer R, Back T, eds. Magnetic resonance imaging in ischemic stroke. Berlin, Germany: Springer, 2005; 239–250.
4. Okamura T, Ishibashi N, Kumar TS, et al. Hypothermic circulatory arrest increases permeability of the blood brain barrier in watershed areas. Ann Thorac Surg 2010;90(6):2001–2008. CrossRef, Medline
5. Kumar R, Woo MA, Macey PM, Fonarow GC, Hamilton MA, Harper RM. Brain axonal and myelin evaluation in heart failure. J Neurol Sci 2011;307(1-2):106–113. CrossRef, Medline
6. Song SK, Sun SW, Ramsbottom MJ, Chang C, Russell J, Cross AH. Dysmyelination revealed through MRI as increased radial (but unchanged axial) diffusion of water. Neuroimage 2002;17(3):1429–1436. CrossRef, Medline
7. Alexander AL, Lee JE, Lazar M, Field AS. Diffusion tensor imaging of the brain. Neurotherapeutics 2007;4(3):316–329. CrossRef, Medline
8. Xie M, Tobin JE, Budde MD, et al. Rostrocaudal analysis of corpus callosum demyelination and axon damage across disease stages refines diffusion tensor imaging correlations with pathological features. J Neuropathol Exp Neurol 2010;69(7):704–716. CrossRef, Medline
9. Beaulieu C. The basis of anisotropic water diffusion in the nervous system: a technical review. NMR Biomed 2002;15(7-8):435–455. CrossRef, Medline
10. Mac Donald CL, Dikranian K, Bayly P, Holtzman D, Brody D. Diffusion tensor imaging reliably detects experimental traumatic axonal injury and indicates approximate time of injury. J Neurosci 2007;27(44):11869–11876. CrossRef, Medline
11. Mac Donald CL, Dikranian K, Song SK, Bayly PV, Holtzman DM, Brody DL. Detection of traumatic axonal injury with diffusion tensor imaging in a mouse model of traumatic brain injury. Exp Neurol 2007;205(1):116–131. CrossRef, Medline
12. Song SK, Sun SW, Ju WK, Lin SJ, Cross AH, Neufeld AH. Diffusion tensor imaging detects and differentiates axon and myelin degeneration in mouse optic nerve after retinal ischemia. Neuroimage 2003;20(3):1714–1722. CrossRef, Medline
13. Sun SW, Liang HF, Trinkaus K, Cross AH, Armstrong RC, Song SK. Noninvasive detection of cuprizone induced axonal damage and demyelination in the mouse corpus callosum. Magn Reson Med 2006;55(2):302–308. CrossRef, Medline
14. Takahashi M, Ono J, Harada K, Maeda M, Hackney DB. Diffusional anisotropy in cranial nerves with maturation: quantitative evaluation with diffusion MR imaging in rats. Radiology 2000;216(3):881–885. Abstract, Medline
15. Song SK, Yoshino J, Le TQ, et al. Demyelination increases radial diffusivity in corpus callosum of mouse brain. Neuroimage 2005;26(1):132–140. CrossRef, Medline
16. Luyt CE, Galanaud D, Perlbarg V, et al. Diffusion tensor imaging to predict long-term outcome after cardiac arrest: a bicentric pilot study. Anesthesiology 2012;117(6):1311–1321. CrossRef, Medline
17. Galanaud D, Perlbarg V, Gupta R, et al. Assessment of white matter injury and outcome in severe brain trauma: a prospective multicenter cohort. Anesthesiology 2012;117(6):1300–1310. CrossRef, Medline
18. Jennett B, Bond M. Assessment of outcome after severe brain damage. Lancet 1975;1(7905):480–484. CrossRef, Medline
19. Marshall LF, Marshall SB, Klauber MR, et al. The diagnosis of head injury requires a classification based on computed axial tomography. J Neurotrauma 1992;9(suppl 1):S287–S292. Medline

20. Mori S, Oishi K, Jiang H, et al. Stereotaxic white matter atlas based on diffusion tensor imaging in an ICBM template. Neuroimage 2008;40:570–582. CrossRef, Medline
21. Lennon VA, Whittingham S, Carnegie PR, McPherson TA, Mackay IR. Detection of antibodies to the basic protein of human myelin by radioimmunoassay and immunofluorescence. J Immunol 1971;107(1):56–62. Medline
22. Sharma HS, Zimmer C, Westman J, Cervós-Navarro J. Acute systemic heat stress increases glial fibrillary acidic protein immunoreactivity in brain: experimental observations in conscious normotensive young rats. Neuroscience 1992;48(4):889–901. CrossRef, Medline
23. Sharma HS, Kretzschmar R, Cervós-Navarro J, Ermisch A, Rühle HJ, Dey PK. Age-related pathophysiology of the blood-brain barrier in heat stress. Prog Brain Res 1992;91:189–196. CrossRef, Medline
24. Sharma HS, Olsson Y, Cervós-Navarro J. p-Chlorophenylalanine, a serotonin synthesis inhibitor, reduces the response of glial fibrillary acidic protein induced by trauma to the spinal cord: an immunohistochemical investigation in the rat. Acta Neuropathol (Berl) 1993;86(5):422–427. CrossRef, Medline
25. Sharma HS, Miclescu A, Wiklund L. Cardiac arrest-induced regional blood-brain barrier breakdown, edema formation and brain pathology: a light and electron microscopic study on a new model for neurodegeneration and neuroprotection in porcine brain. J Neural Transm 2011;118(1):87–114. CrossRef, Medline
26. Miller JR, Myers RE. Neuropathology of systemic circulatory arrest in adult monkeys. Neurology 1972;22(9):888–904. CrossRef, Medline
27. Ginsberg MD, Myers RE. The topography of impaired microvascular perfusion in the primate brain following total circulatory arrest. Neurology 1972;22(10):998–1011. CrossRef, Medline
28. Ginsberg MD, Hedley-Whyte ET, Richardson EP Jr. Hypoxic-ischemic leukoencephalopathy in man. Arch Neurol 1976;33(1):5–14. CrossRef, Medline
29. Busl KM, Greer DM. Hypoxic-ischemic brain injury: pathophysiology, neuropathology and mechanisms. NeuroRehabilitation 2010;26(1):5–13. Medline
30. Ommaya AK, Gennarelli TA. Cerebral concussion and traumatic unconsciousness: correlation of experimental and clinical observations of blunt head injuries. Brain 1974;97(4):633–654. CrossRef, Medline
31. Sidaros A, Engberg AW, Sidaros K, et al. Diffusion tensor imaging during recovery from severe traumatic brain injury and relation to clinical outcome: a longitudinal study. Brain 2008;131(Pt 2):559–572. CrossRef, Medline
32. Le TH, Mukherjee P, Henry RG, Berman JI, Ware M, Manley GT. Diffusion tensor imaging with three-dimensional fiber tractography of traumatic axonal shearing injury: an imaging correlate for the posterior callosal “disconnection” syndrome—case report. Neurosurgery 2005;56(1):189. Medline
33. Arfanakis K, Haughton VM, Carew JD, Rogers BP, Dempsey RJ, Meyerand ME. Diffusion tensor MR imaging in diffuse axonal injury. AJNR Am J Neuroradiol 2002;23(5):794–802. Medline
34. Newcombe VF, Williams GB, Nortje J, et al. Analysis of acute traumatic axonal injury using diffusion tensor imaging. Br J Neurosurg 2007;21(4):340–348. CrossRef, Medline
35. Nakayama N, Okumura A, Shinoda J, et al. Evidence for white matter disruption in traumatic brain injury without macroscopic lesions. J Neurol Neurosurg Psychiatry 2006;77(7):850–855. CrossRef, Medline
36. Ptak T, Sheridan RL, Rhea JT, et al. Cerebral fractional anisotropy score in trauma patients: a new indicator of white matter injury after trauma. AJR Am J Roentgenol 2003;181(5):1401–1407. CrossRef, Medline
37. Kumar R, Saksena S, Husain M, et al. Serial changes in diffusion tensor imaging metrics of corpus callosum in moderate traumatic brain injury patients and their correlation with neuropsychometric tests: a 2-year follow-up study. J Head Trauma Rehabil 2010;25(1):31–42. CrossRef, Medline
38. Inglese M, Makani S, Johnson G, et al. Diffuse axonal injury in mild traumatic brain injury: a diffusion tensor imaging study. J Neurosurg 2005;103(2):298–303. CrossRef, Medline
39. Huisman TA, Schwamm LH, Schaefer PW, et al. Diffusion tensor imaging as potential biomarker of white matter injury in diffuse axonal injury. AJNR Am J Neuroradiol 2004;25(3):370–376. Medline
40. Newcombe VF, Williams GB, Scoffings D, et al. Aetiological differences in neuroanatomy of the vegetative state: insights from diffusion tensor imaging and functional implications. J Neurol Neurosurg Psychiatry 2010;81(5):552–561. CrossRef, Medline
41. Parvizi J, Damasio AR. Neuroanatomical correlates of brainstem coma. Brain 2003;126(pt 7):1524–1536. CrossRef, Medline
42. Weiss N, Galanaud D, Carpentier A, Naccache L, Puybasset L. Clinical review: prognostic value of magnetic resonance imaging in acute brain injury and coma. Crit Care 2007;11(5):230. CrossRef, Medline